Convulxin Forms a Dimer in Solution and Can Bind Eight Copies of Glycoprotein VI: Implications for Platelet Activation[†]

Katsunori Horii,[‡] Monica T. Brooks, and Andrew B. Herr*

Department of Molecular Genetics, Biochemistry and Microbiology, University of Cincinnati College of Medicine, Cincinnati, Ohio 45267-0524

Received September 24, 2008; Revised Manuscript Received January 16, 2009

ABSTRACT: Convulxin (CVX) is a C-type lectin-like protein from the venom of the South American rattlesnake that functions as a potent agonist of the platelet collagen receptor glycoprotein VI (GPVI). Although CVX is widely used as a platelet agonist, the molecular basis for its extremely high potency is not clear. In order to delineate possible mechanisms for CVX-induced GPVI activation, we used analytical ultracentrifugation to determine the assembly state of CVX in solution and surface plasmon resonance in order to understand the affinity, kinetics, and stoichiometry of GPVI binding to CVX. We show here that CVX exists in solution as a dimer of $\alpha_4\beta_4$ rings, yielding eight potential binding sites for GPVI. Binding studies confirm that all eight sites are able to bind GPVI tightly, each with high picomolar or low nanomolar affinity. Reanalysis of previously determined crystal structures of CVX revealed the dimer in both structures. The dimeric nature of CVX and its ability to bind eight GPVI molecules suggest that it might be capable of binding to GPVI expressed on two opposing surfaces. Agglutination assays using GPVI-coated beads confirm that CVX is able to bridge distinct GPVI-coated surfaces and indicate that CVX agglutination of platelets is dependent on GPVI binding. Thus, in addition to clustering up to eight GPVI receptors, CVX may facilitate platelet activation by bridging platelets directly.

Platelet activation in response to collagen requires glycoprotein VI (GPVI)[1] (*1, 2*), a multichain immune-type receptor (*3*). Although the physiological ligand for GPVI is fibrous collagen, collagen-related peptides (CRP) and various snake venom proteins are capable of triggering platelet activation via GPVI (*4*−*6*). The best characterized GPVI agonist from snake venom is CVX, a C-type lectin-like protein (CLP) from the venom of the South American rattlesnake *Crotalus durissus terrificus* that forms a disulfide-linked $\alpha_4\beta_4$ heterooctameric ring (*7*−*12*). CVX is a very potent platelet activator, with an effective dose (ED_{50}) of only 200 pM (*13*). It is assumed that the potent agonist activity of CVX is due to some combination of its high affinity for GPVI and/or its stoichiometry of interaction with GPVI, but detailed quantitative analyses of the affinity and kinetics of binding at a single site or receptor stoichiometry are lacking. Here we use a combination of analytical ultracentrifugation and surface plasmon resonance to show that CVX exists in solution as a dimer of $\alpha_4\beta_4$ rings, that CVX has eight distinct GPVI binding sites, and that each site binds with very high (picomolar to low nanomolar) affinity. Furthermore, bead agglutination assays show that the presence of two distinct GPVI-binding surfaces on the $(\alpha_4\beta_4)_2$ CVX dimer allows CVX to both cluster GPVI on a single cell and to cross-link target cells via GPVI.

EXPERIMENTAL PROCEDURES

Expression and Purification of GPVI, GPVI-Fcα, and CVX. The collagen-binding domain (CBD) of human GPVI was expressed, refolded, and purified as described (*14*). The GPVI-Fcα fusion construct was made by subcloning the GPVI CBD into a pcDNA3 expression vector containing a human IgA1-Fc fragment (*15*), with an intervening $(Gly\text{-}Ser)_3$ linker. The construct included a rat IgG2b secretion signal and a C-terminal factor Xa cleavage site and hexahistidine tag. COS-7 cells were grown to confluence and transiently transfected with the GPVI-Fcα vector. Secreted GPVI-Fcα fusion protein was purified from media by Ni-NTA and gel filtration chromatography as described for the parent IgA1-Fc protein (*15*).

Approximately 250 mg of freeze-dried venom from *C. durissus terrificus* (Miami Serpentarium) was resuspended in 5 mL of TBS (20 mM Tris-HCl, pH 7.4, 150 mM NaCl) with complete protease inhibitor cocktail tablet (Roche) and spun down at 10000 rpm for 20 min. The supernatant was passed through a HiTrap benzamidine FF (high sub) 5 mL column (GE Healthcare) to remove serine proteases and further purified by gel filtration using a HiLoad Superdex 200 16/60 (GE Helthcare) column. All proteins were judged to be >95% pure by SDS−PAGE. Extinction coefficients were calculated based on sequence using the ProtParam tool

[†] This work was supported by an American Heart Association Scientist Development Grant and funds from the State of Ohio Eminent Scholar Program to A.B.H.

* To whom correspondence should be addressed. Phone: 513-558-5312. Fax: 513-558-1190. E-mail: Andrew.Herr@UC.edu.

[‡] Current address: VALWAY Technology Center, NEC Soft, Ltd., Tokyo 136-8627, Japan.

[1] Abbreviations: CVX, convulxin; GPVI, glycoprotein VI; AUC, analytical ultracentrifugation; SPR, surface plasmon resonance; CRP, collagen-related peptide; CLP, C-type lectin-like protein; ED_{50}, effective dose; CBD, collagen-binding domain; TBS, Tris-buffered saline; PBS, phosphate-buffered saline; RU, response unit.

10.1021/bi801820q CCC: $40.75
Published on Web 02/11/2009

Table 1: Sedimentation Analysis of the CVX Dimer in Solution

	sedimentation velocity analysis			sedimentation equilibrium analysis		
species	s^* (S)	f/f_0	M_{app} (g/mol)	σ^a (cm^{-2})	dimer $M_{sequence}$ (g/mol)	M_{exptl} (g/mol)
dimer $(\alpha_4\beta_4)_2$	9.79	1.47	253800 ± 14900	2.922	245085	237300 (226700−248300)[b]

[a] σ is the experimental reduced buoyant molecular mass, reported at 10000 rpm. [b] Values in parentheses represent the 95% confidence interval.

Table 2: SPR Kinetic and Equilibrium Binding Parameters

[NaCl] (M)	k_{MT} (s^{-1})	$k_{on}1$ (M^{-1} s^{-1})[a]	$k_{off}1$ (s^{-1})	$k_{on}2$ (M^{-1} s^{-1})	$k_{off}2$ (s^{-1})[a]	K_D1 (nM)	K_D2 (nM)
Kinetic Analysis at 100 μL/min; Global Fit of Three Flow Cells (28 Curves) with Bivalent Ligand Model							
0.3	n/a	6.10×10^5	7.15×10^{-4}	5.81×10^5	5.40×10^{-3}	1.18 ± 0.01	9.31 ± 0.07
Kinetic Analysis at 30 μL/min; Bivalent Ligand with Mass Transport Model							
0.1	1.75×10^8	4.36×10^5	2.68×10^{-4}	1.25×10^7	1.62×10^{-2}	0.616 ± 0.004	1.29 ± 0.07
0.15	1.75×10^8	6.30×10^5	5.09×10^{-4}	2.11×10^6	6.90×10^{-3}	0.807 ± 0.004	3.27 ± 0.05
0.3	1.75×10^8	4.00×10^5	7.09×10^{-4}	7.76×10^5	8.15×10^{-3}	1.78 ± 0.005	10.5 ± 0.1
1	1.75×10^8	2.28×10^5	6.75×10^{-4}	2.02×10^5	5.60×10^{-3}	2.97 ± 0.01	27.7 ± 0.4
Equilibrium Analysis of Steady-State Data Using a Two-Site Binding Model							
0.3						1.07 ± 0.05	17.0 ± 2.1
1						1.73 ± 0.04	48.1 ± 3.6

[a] Rate constants $k_{on}1$ and $k_{off}2$ have been corrected by statistical factors, as described in Experimental Procedures. Kinetic rate constants were determined using the program ClampXP. Equilibrium constants derived for steady-state data were determined using the program Scientist.

on the Expasy server (http://expasy.org) to be 33140 M^{-1} for GPVI, 151080 M^{-1} for dimeric GPVI-Fcα, and 373560 M^{-1} (i.e., 93390 M^{-1} for $\alpha\beta$ heterodimer) for the $\alpha_4\beta_4$ heterooctamer of CVX.

Analytical Ultracentrifugation. Sedimentation velocity and equilibrium experiments were carried out using absorbance optics on a Beckman XL-I analytical ultracentrifuge. For sedimentation velocity experiments, 400 μL samples of CVX in TBS at concentrations ranging from 104.8 to 582 nM (molar units are listed for the $\alpha_4\beta_4$ heterooctamer) were spun overnight at 36000 rpm at 20 °C (*14, 16*). The sedimentation coefficient distribution was determined using the program SEDFIT (*17*). Mixing GPVI with CVX at neutral pH resulted in massive aggregation of the complex, which precluded analysis under these conditions. For sedimentation equilibrium experiments, CVX samples in phosphate-buffered saline (PBS) at 5.4, 26.7, and 134 nM were spun at 10000, 12000, 14000, and 20000 rpm until equilibrium was reached. The use of PBS allowed us to maximize sensitivity and scan at low wavelengths of 210, 230, and 280 nm. Equilibrium data were trimmed using WinREEDIT and globally analyzed with the program WinNONLIN (http://www.rasmb.bbri.org/), and experimental molecular mass was determined as described (*16, 18*) (Table 1). Although CVX is potentially O-glycosylated (*7*), the predicted glycosylation would only contribute ~1% of the total mass and was thus assumed to be negligible when calculating the partial specific volume and experimental molecular mass.

Surface Plasmon Resonance Spectroscopy. Kinetic and equilibrium binding experiments were carried out using a Biacore 3000 surface plasmon resonance (SPR) instrument. CVX was covalently coupled to research grade CM5 chips using standard random amine coupling, with coupling densities ranging from 60 to 8000 response units (RUs). Serial 2-fold dilutions of GPVI from 200 nM down to 195 pM in TBS with 0.005% P-20 were injected at a flow rate of 30 μL/min. Kinetic data measured at 0.1, 0.15, 0.3, and 1 M NaCl were analyzed with the program ClampXP (*19*) using single-site, bivalent ligand, and tetravalent ligand binding models. The data were best described by the bivalent ligand model, indicating that two classes of binding sites exist on CVX. The data collected at lower NaCl concentrations showed strong evidence of mass transport-limited binding. Thus, the kinetic data were analyzed using a bivalent ligand model with mass transport; the rate of diffusion was fixed at 1.75×10^8 s^{-1} (*20*). The apparent kinetic rate constants reported by ClampXP were corrected by appropriate statistical factors (i.e., the corrected value $k_{on}1 = 0.5k_{on,app}1$ as derived from ClampXP; corrected $k_{off}2 = 0.5k_{off,app}2$), as described (*15, 16*). Steady-state binding curves were generated by injecting GPVI at a low flow rate of 5 μL/min for long time periods (3000 s) in order to reach equilibrium. The flat plateaus of each binding curve at equilibrium were averaged; these equilibrium binding isotherms were fitted to a two-site binding model using the program Scientist (Micromath, Salt Lake City, UT) with the equation:

$$R_{eq} = \frac{R_{max}(K_1x + K_2x + 2K_1K_2x^2)}{2(1 + K_1x + K_2x + K_1K_2x^2)}$$

where R_{eq} is the equilibrium binding response at a given free analyte concentration x, R_{max} is the maximum binding response (i.e., RU value for full saturation), and K_1 and K_2 are the association equilibrium constants (i.e., $1/K_D1$ and $1/K_D2$) for the first and second binding events, respectively. For determination of the electrostatic contribution of binding, the logarithm of the association equilibrium constant (i.e., $1/K_D$) was plotted versus the logarithm of NaCl concentration. The slope of this plot yields SK_{obs}, the net number of Na^+ and Cl^- ions bound or released upon complex formation (*23*). The magnitude of this slope is an indicator of the extent to which electrostatics dominate a binding reaction. The association equilibrium constants measured at each NaCl concentration (see Table 2) were converted to ΔG values according to the relation $\Delta G = -RT \ln K$. ΔG values determined at 150 mM and 1 M NaCl were compared in order to determine the contribution of electrostatics to the free energy of binding.

Dynabead Agglutination Assays. Co-NTA-coated Dynabeads (50 μL) with 1 μM diameter (Invitrogen) were incubated with 15 μg of GPVI-Fcα overnight at 4 °C. After resuspending in TBS, GPVI-Fcα-coated beads were incubated with 3-fold dilutions of CVX ranging from 10.3 pM to 67.5 nM and visualized in a 96-well plate using an Olympus SZ60 stereoscope equipped with an Olympus C5050z digital camera. Bead agglutination was quantitated using the Java program ImageJ (http://rsb.info.nih.gov/ij/index.html). The Subtract Background command was applied to each image using a sliding paraboloid with apex curvature equivalent to a sphere with a radius of 255 pixels. Each image was inverted, and the Otsu threshold plugin (http://www.uhnresearch.ca/facilities/wcif/fdownload.html) was used to select the bead aggregates, followed by quantitation using the Analyze Particles command.

RESULTS

CVX Forms a Dimer of $\alpha_4\beta_4$ Rings in Solution. Purified CVX migrated as a doublet of bands at 13−14 kDa by reducing SDS−PAGE, and a single band at ~110 kDa by nonreducing SDS−PAGE, as previously described (*10, 11*). The ~110 kDa size is consistent with the $\alpha_4\beta_4$ heterooctameric assembly revealed in two independent crystal structures of CVX (*8, 9*). However, when we characterized its hydrodynamic behavior in solution by analytical ultracentrifugation (AUC), sedimentation velocity experiments revealed that CVX sedimented at 9.8 S, with an estimated molecular mass of approximately 245 kDa (Figure 1A, Table 1). The sedimentation velocity results suggested that CVX was likely sedimenting as a dimer of $\alpha_4\beta_4$ rings in solution. Additional minor peaks were observed at 6.4 and 14.2 S that likely correspond to a single $\alpha_4\beta_4$ ring or a higher order oligomer, respectively; however, each of these peaks was less than 1.5% of the height of the major peak. Additional velocity runs at lower concentrations showed both 6.4 and 9.8 S peaks at similar ratios but did not exhibit the putative higher order oligomer at 14.2 S. To verify the assembly state of CVX, we carried out sedimentation equilibrium experiments using loading concentrations ranging from 5.4 to 134 nM, which upon equilibration resulted in experimental concentrations between 1 nM and 3 μM. The data could be fitted by a single species with a molecular mass of 237 kDa, corresponding to an $(\alpha_4\beta_4)_2$ dimer (Figure 1B, Table 1). Upon further analysis of the two independent crystal structures of CVX, both showed that CVX formed a back-back dimer of $\alpha_4\beta_4$ rings in the asymmetric unit, consistent with our result in solution (Figure 1C) (*8, 9*). Our results represent the first demonstration that CVX forms a dimer in solution even at very low nanomolar concentrations, which is in the same concentration regime over which CVX activates platelets (*13*).

CVX Binds GPVI at Multiple Sites, Each with High Affinity. In order to determine the affinity, kinetics, and stoichiometry of the interaction between GPVI and CVX, we performed SPR analyses of the binding of soluble GPVI ectodomain to CVX. The experimental orientation used, with the multivalent protein (CVX) coupled to the chip and the monomeric protein (GPVI) flowed over, yields the most accurate equilibrium constants for individual binding events, without the complication of avidity effects (*15, 16*). Kinetic and equilibrium analyses were carried out; in both cases the data were best described by two classes of binding sites with different K_Ds (Figure 2). Data collected at lower NaCl concentrations at 30 μL/min showed evidence of mass

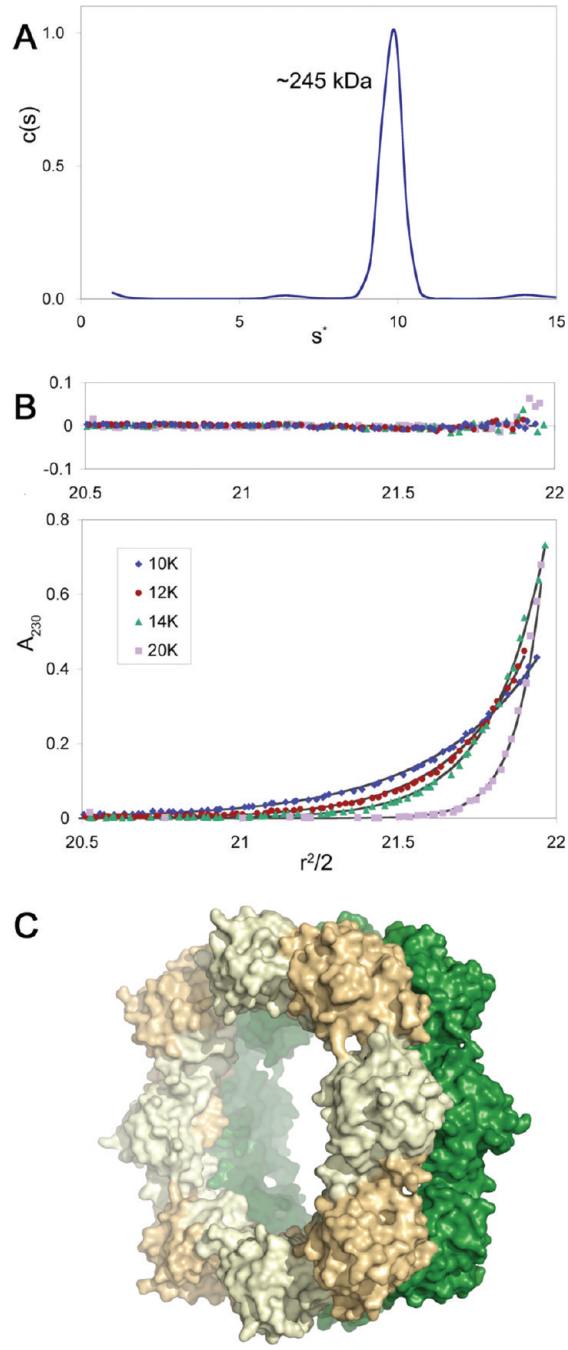

FIGURE 1: CVX exists in solution as an $(\alpha_4\beta_4)_2$ dimer. (A) Sedimentation coefficient distribution of CVX from a sedimentation velocity AUC experiment. CVX was spun at 36000 rpm at 20 °C in a Beckman XL-I analytical ultracentrifuge and analyzed using the *c*(*s*) model in Sedfit. After fitting the frictional ratio, the *c*(*M*) model was used to estimate the molecular mass. CVX sediments as a single species with an estimated molecular mass consistent with a dimer. (B) Representative curves and associated residuals from a sedimentation equilibrium AUC experiment. A total of 12 data curves from three loading concentrations (5.4−134 nM) and four speeds (10K, 12K, 14K, and 20K rpm) were globally fitted using the program WinNONLIN. The data described a single dimeric species with an experimental molecular mass of 237 kDa. (C) Structure of the CVX dimer taken from PDB 1UMR (*8*). One $\alpha_4\beta_4$ ring is shown in shades of light brown, with α and β subunits colored differently. The second $\alpha_4\beta_4$ ring is shown in green.

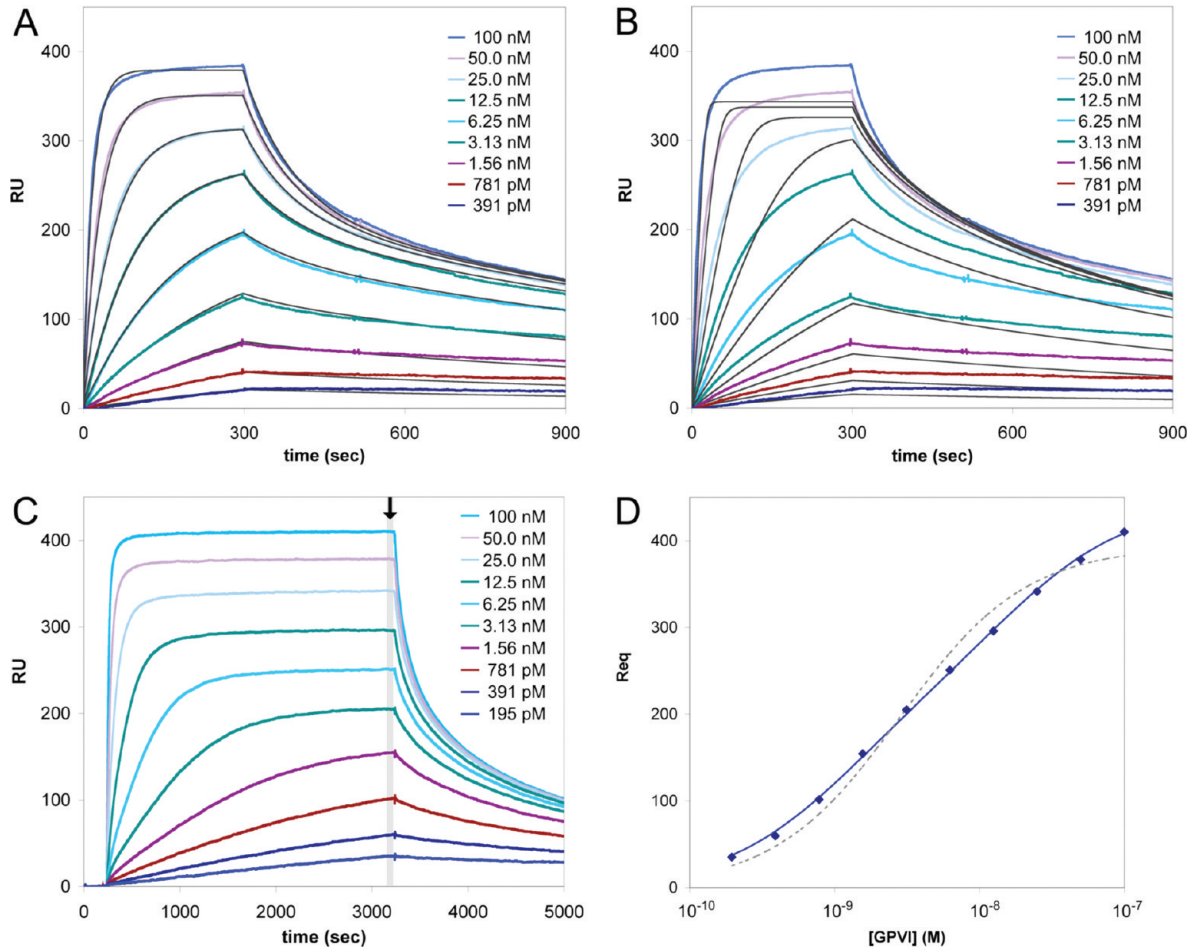

FIGURE 2: GPVI binds individual sites on CVX with very high affinity. (A) Representative kinetic SPR data from injections of soluble GPVI over CVX coupled to a CM5 chip, carried out at 300 mM NaCl. Data were fitted to a mass transport-limited bivalent ligand model (i.e., two classes of binding sites on CVX) using the program ClampXP, with the resulting kinetic and equilibrium constants listed in Table 2. Raw data curves are shown in color according to the injected GPVI concentrations; fits to the two-site model are shown in black. (B) The same raw data shown in panel A but fitted instead to a mass transport-limited single-site binding model. The poor fits to the data indicate that two classes of binding sites must be incorporated into the binding model (as in panel A) in order to accurately describe the data. (C) Representative steady-state SPR data from long injections of GPVI over CVX at a 5 μL/min flow rate. The equilibrium binding response was calculated by averaging the response over a 60 s time period at the plateau. The range of data used for the averaging procedure is illustrated by the vertical gray stripe and highlighted by the black arrow. (D) Equilibrium SPR binding isotherms for soluble GPVI injected over CVX. Average binding responses at steady state from panel C were plotted as a function of injected GPVI concentration. The continuous blue line shows the fit using a two-site model in the program Scientist, yielding affinities similar to those determined by kinetic experiments. The gray dashed line shows the fit using a single-site model for comparison.

transport (*21*). This occurs when the on-rates for protein−protein interaction are fast enough to deplete the region above the chip of analyte faster than it is replenished by bulk flow. These data were therefore fitted using a mass transport-linked bivalent ligand model; for comparison, data were collected at 300 mM NaCl at a flow rate of 100 μL/min, where mass transport was minimal (Figure 2A). The kinetic rate constants and derived equilibrium constants were similar in both cases (Table 2). The on-rates for binding of GPVI to CVX were fast (4.6×10^5 to 1.3×10^6 M^{-1} s^{-1} for the first binding event), with relatively slow dissociation kinetics (2.7×10^{-4} to 7.2×10^{-4} s^{-1} for the first binding event). Each individual GPVI receptor bound tightly, with affinities of 0.807 and 3.27 nM for the first and second binding events at 150 mM NaCl. Equilibrium affinity constants determined by steady-state analyses confirmed the equilibrium constants derived from kinetic data under the same conditions (Figure 2C,D, Table 2).

The Role of Electrostatics in the GPVI−CVX Interaction. The crystal structure of CVX revealed a negatively charged patch on its surface in a region likely to contain the GPVI-binding site, based on related C-type lectin-like proteins (CLP) such as factor X-binding protein (*22*). Furthermore, the structure of GPVI exhibits a positively charged region surrounding the putative collagen-binding groove, consisting of residues K41, K59, R60, and R169 (*14*). It was suggested that charge complementarity may play a role in the binding of GPVI to CVX (*9*). To address the importance of electrostatics in the GPVI−CVX complex, we analyzed the NaCl dependence of binding. The binding of GPVI to CVX became weaker at higher NaCl concentrations; plotting the logarithms of the association equilibrium constants ($K_A = 1/K_D$) versus log [NaCl] yielded values for the slope (called SK_{obs}) of −0.70 or −1.3 for the higher and lower affinity classes of binding sites, respectively (Figure 3A). SK_{obs} corresponds to the net gain or loss of Na^+ and Cl^- ions when GPVI binds CVX; the magnitude of SK_{obs} is correlated to the electrostatic component of binding (*23*). These results indicate that although electrostatics do play a role in the interaction, the majority of the free energy of binding is

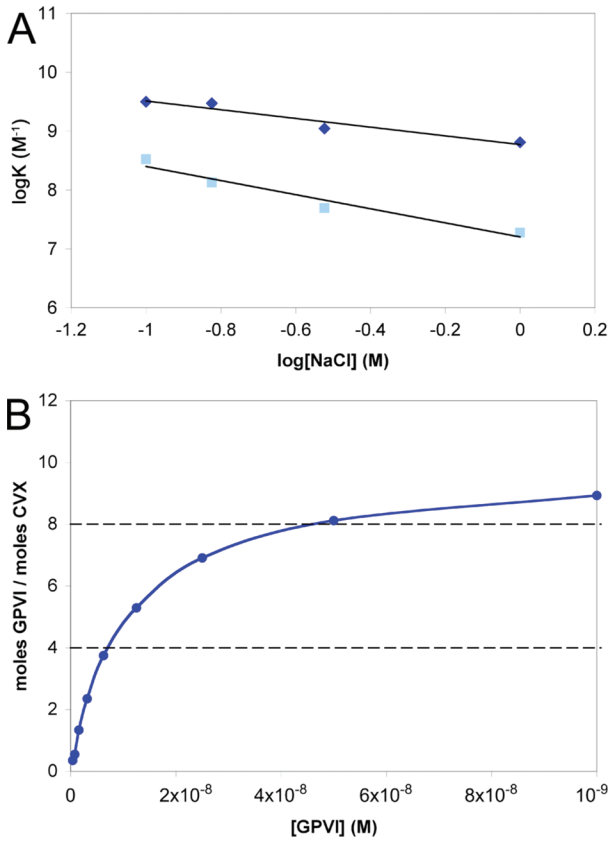

FIGURE 3: Analysis of the electrostatic component and stoichiometry of the GPVI−CVX interaction. (A) Logarithmic plot of the association equilibrium constants derived from kinetic experiments versus NaCl concentration. The slope of this plot, SK_{obs}, is an indicator of the degree to which electrostatics govern the binding interaction. Diamonds and squares illustrate the first and second binding events, with SK_{obs} values of −0.70 and −1.3, respectively. Only ~10% of the free energy of binding is contributed by electrostatic interactions. (B) Plot of the number of moles of GPVI bound per mole of CVX dimer. The data from four experiments spanning a range of coupling densities were averaged. The data are consistent with four GPVI molecules binding to each $\alpha_4\beta_4$ ring, for a total of eight per CVX dimer.

derived from other sources, such as hydrogen bonding, van der Waals interactions, and burial of hydrophobic surfaces. Comparison of the free energy of binding (ΔG) at 150 mM versus 1 M NaCl (where electrostatic interactions are negligible due to screening by the salt (*24*)) reveals that only 7−11% of the total binding free energy is due to electrostatic contributions.

Eight GPVI Molecules Bind Each $(\alpha_4\beta_4)_2$ CVX Dimer. Given that each $\alpha_4\beta_4$ CVX ring has 4-fold symmetry and that our data reveal that CVX forms a stacked dimer in solution, it is of significant interest to understand the stoichiometry of the GPVI−CVX interaction. It has been assumed that four GPVI receptors bind to each $\alpha_4\beta_4$ ring, but no experimental evidence has been presented to verify this. In SPR, the response units (RUs) observed are proportional to the mass of injected analyte bound to the ligand on the chip surface. Using the known molecular masses of the CVX dimer and GPVI, combined with the coupling density of CVX, the stoichiometry of binding can be determined. The GPVI binding responses at four different CVX coupling densities were plotted as moles of bound GPVI per moles of coupled CVX (Figure 3B). After averaging, the stoichiometry of the complex is between eight and nine GPVI molecules bound per CVX $(\alpha_4\beta_4)_2$ dimer. Thus, these results are consistent with the binding of four GPVI receptors to each $\alpha_4\beta_4$ CVX ring, yielding at least eight GPVI receptor sites on the CVX dimer, each of which exhibits high picomolar to low nanomolar affinity. It should be noted that AUC experiments to verify the stoichiometry were precluded due to pronounced aggregation of the GPVI−CVX complex when mixed in a stoichiometric ratio, even at concentrations less than 0.1 mg/mL. This phenomenon suggests that the interaction of soluble GPVI with CVX leads to higher order assembly of the complex, to the extent that little remains in solution. It is possible that this higher order assembly might involve the binding of additional GPVI molecules with lower affinity to yield even higher stoichiometries.

CVX Can Bridge GPVI on Opposing Surfaces. The dimeric nature of CVX and its ability to bind eight GPVI receptors simultaneously suggest that CVX should be capable of agglutination of platelets via GPVI interactions. CVX-mediated agglutination of fixed platelets has previously been shown to occur at 2 μg/mL CVX (equivalent to 8 nM dimeric CVX) (*25*) but not at lower concentrations sufficient to induce activation (*10*). Furthermore, it is not yet clear whether CVX-mediated agglutination is due to interaction with GPVI or GPIbα. To assay the concentration dependence of CVX-mediated agglutination and to avoid experimental complications of cell activation or alternate receptors for CVX, we carried out a GPVI-coated bead agglutination assay. Cobalt-NTA-coated polystyrene beads (Dynabeads) were coated with a hexahistidine-tagged GPVI-Fcα fusion protein. Upon incubation with varying concentrations of CVX, beads showed appreciable agglutination at CVX concentrations above 833 pM, and agglutination became pronounced at nanomolar concentrations. The CVX concentration range over which agglutination occurs coincides with the K_D values for individual sites determined in this study (Figure 4). The agglutination results confirm the hypothesis that CVX is able to simultaneously bind to GPVI molecules on two distinct surfaces and could thus bridge platelets.

DISCUSSION

Due to its potent agonism (*10, 13*), CVX has become the *de facto* gold standard for measuring platelet activation. Both fibrous collagen and CVX trigger platelet activation by initiating clustering of GPVI and the associated FcR γ-chain signaling coreceptor. However, there are significant differences in the degree and kinetics of activation. Previous work by the Kahn laboratory showed that RBL cells transfected with GPVI could be activated by CVX but required a receptor surface density approximating that found on platelets in order to be activated by collagen (*27, 28*). This phenomenon may be due to GPVI dimerization at sufficient receptor densities that increases its affinity for collagen (*14, 29, 30*). In contrast, Tomlinson et al. found no threshold effect for collagen signaling through GPVI when using a transfected DT40 model B-cell line (*26*). Their data revealed that collagen induces a delayed low-level activation response that persists for an extended period, which may be important for platelet spreading on a collagen substrate. In contrast, CVX triggers rapid and strong but transient activation (*26*). The inhibitory collagen receptor LAIR-1, which is expressed on RBL cells but not DT40 cells (and not on platelets), was shown to inhibit collagen-mediated activation via GPVI,

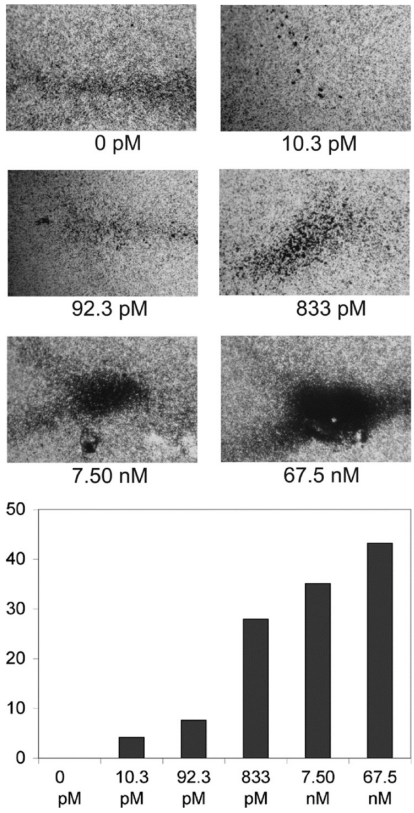

FIGURE 4: Concentration-dependent agglutination of GPVI-coated Dynabeads by CVX. Hexahistidine-tagged GPVI-Fcα was captured on the surface of Co-NTA-coated Dynabeads with 1 μm diameter. Addition of CVX to GPVI-Dynabeads induced agglutination at CVX concentrations in the high picomolar and nanomolar range. Clustering became noticeable at 833 pM and increased at nanomolar CVX concentrations. These values correspond to the K_D values reported here for GPVI binding to individual sites on CVX. Unmodified Dynabeads (i.e., without captured GPVI) showed no agglutination even at the highest CVX concentration. The bar graph shows the mean intensities of the bead clusters on an arbitrary scale as quantitated by ImageJ after subtracting the intensity value for the beads in the absence of CVX.

possibly explaining the threshold effect of collagen signaling in RBL cells. Regardless of the differences between cell lines, it is clear that collagen and CVX trigger very different responses via the same GPVI receptor.

The underlying differences between the activation of platelets by collagen and CVX likely result from differences in the way each ligand interacts with GPVI. In particular, these factors include (1) affinity and kinetics of binding to GPVI, (2) orientation of the activated receptor cluster upon ligand binding, and (3) stoichiometry of the GPVI−ligand complexes. It has been clear for many years that CVX binds GPVI with high macroscopic affinity, based on studies of radiolabeled or fluorescently labeled CVX binding to platelets (*10, 13, 31*). The macroscopic affinity results from the multivalent interaction of multiple GPVI molecules with CVX as opposed to the interaction of GPVI with individual sites on CVX (*32*). Our results indicate that even when comparing the affinity of a single GPVI receptor for the ligand, CVX has a much higher GPVI-binding affinity than collagen or CRP. At 150 mM NaCl, we find that a single GPVI binds CVX with a K_D of 0.8−3 nM, compared to a 5 μM K_D for soluble CRP (*14*). Binding of monomeric GPVI to fibrous collagen is essentially undetectable, although a dimeric GPVI-Fc construct binds immobilized collagen with a K_D of 576 nM (*33*). Thus, GPVI binds to CVX 200−6000-fold more tightly than to collagen or CRP. Our kinetic analyses reveal that individual GPVI molecules bind to CVX with fast on-rates and slow off-rates, consistent with the high affinity of binding. The on-rate for GPVI binding CVX is 30−100-fold faster than the association of GPVI with collagen or CRP (*33*), and the dissociation was 50−100 times slower than dissociation from CRP and about 10 times slower than dissociation from collagen. Based on our observation that four GPVI molecules bind per $\alpha_4\beta_4$ CVX ring, combined with the high affinity, rapid association, and slow dissociation of GPVI, CVX would be very efficient at inducing a GPVI signaling cluster.

The nature of the GPVI cluster induced by CVX and collagen is necessarily quite different. Based on other C-type lectin-like snake venom proteins (i.e., factor X-binding protein bound to the Gla domain of factor X (*22*)), the boundary between the α and β CVX subunits is likely to contain the GPVI-binding site. To better understand potential configurations of a CVX-induced GPVI cluster, we used the ClusPro server (http://nrc.bu.edu/cluster/) (*34*) to dock GPVI onto CVX. Several solutions essentially superimposed and were consistent with published data (i.e., showing D1 and the D1/D2 linker of GPVI (*35*) bound in the cleft between the α and β subunits of CVX) (Figure 5). The putative binding sites for GPVI on CVX are quite widely separated

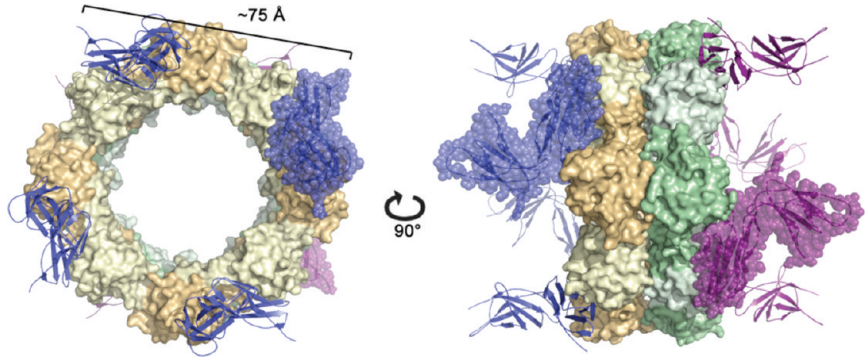

FIGURE 5: Model for GPVI binding to the CVX dimer based on computational docking. The ClusPro server was used to dock GPVI onto a CVX $\alpha\beta$ heterodimer, and symmetry operators were applied to generate the full model of the GPVI−CVX complex. CVX rings are shown in tan and green and docked GPVI molecules in blue and purple. For clarity, one copy of GPVI on each CVX face is illustrated with transparent spheres. Several top solutions resulted in binding topologies similar to that illustrated here, in which the N-terminal domain (D1) and the D1−D2 interface of GPVI are bound in the cleft between α and β subunits of CVX. In this model, the C-termini of adjacent GPVI receptors are ~75 Å apart.

(~110 Å), and our docking analysis suggests that the C-termini of the bound GPVI receptors would be separated by ~75 Å, which may not allow for tight clustering of GPVI. However, we observed dramatic aggregation and precipitation when CVX was mixed with soluble GPVI, suggesting that CVX forms very large higher order assembly states in the presence of soluble GPVI. If such higher order assembly occurs at the cell surface, it could be important in platelet activation, given that large clusters of CVX/GPVI complexes linked together would likely be extremely efficient at triggering a signaling cascade.

In addition to clustering GPVI on a single cell, the dimeric nature of CVX and its ability to bind eight GPVI molecules suggest that CVX could bridge GPVI receptors on adjacent platelets, as confirmed by our Dynabead agglutination assays. This suggests that the extreme potency of CVX as a platelet agonist may result not only from its high affinity for GPVI and its ability to induce GPVI clustering on a single cell but also in its ability to cross-link platelets directly. This would increase the efficiency of platelet aggregation via $\alpha_{IIb}\beta_3$ binding to fibrinogen; furthermore, the close proximity of cross-linked platelets would facilitate platelet activation via secondary mediators released from dense granules. Platelet agglutination has also been observed with other snake venom CLPs (*6*), although those bridge platelets via GPIbα, whereas we demonstrate that interactions with GPVI are responsible for agglutination by CVX. However, CVX also binds GPIbα (*36*), which most likely further potentiates the interaction between GPVI and CVX by helping to localize CVX at the platelet surface.

In contrast to the expected 4-fold symmetry of GPVI when bound to CVX, GPVI has been shown to recognize discrete hydroxyproline-containing motifs scattered infrequently throughout the collagen sequence (*37*). However, the three-dimensional architecture of the intact collagen fiber reveals that adjacent collagen triple helices occur in parallel with the same register, such that the GPVI-binding sequences predominantly form "stripes" that run perpendicular to the main axis of the collagen fiber (*38, 39*). Thus, GPVI clusters induced by fibrous collagen are likely to be linear arrays rather than 4-fold clusters. We hypothesize that the orientation and degree of clustering of GPVI induced by CVX versus collagen are responsible for the differences in the degree and time course of downstream signaling events.

REFERENCES

1. Moroi, M., and Jung, S. M. (2004) Platelet glycoprotein VI: its structure and function. *Thromb. Res. 114*, 221–233.
2. Kahn, M. L. (2004) Platelet-collagen responses: Molecular basis and therapeutic promise. *Semin. Thromb. Hemostasis 30*, 419–425.
3. Clemetson, J. M., Polgar, J., Magnenat, E., Wells, T. N., and Clemetson, K. J. (1999) The platelet collagen receptor glycoprotein VI is a member of the immunoglobulin superfamily closely related to FcαR and the natural killer receptors. *J. Biol. Chem. 274*, 29019–29024.
4. Andrews, R. K., Kamiguti, A. S., Berlanga, O., Leduc, M., Theakston, R. D., and Watson, S. P. (2001) The use of snake venom toxins as tools to study platelet receptors for collagen and von Willebrand factor. *Haemostasis 31*, 155–172.
5. Farndale, R. W., Sixma, J. J., Barnes, M. J., and de Groot, P. G. (2004) The role of collagen in thrombosis and hemostasis. *J. Thromb. Haemostasis 2*, 561–573.
6. Lu, Q., Navdaev, A., Clemetson, J. M., and Clemetson, K. J. (2005) Snake venom C-type lectins interacting with platelet receptors. Structure-function relationships and effects on haemostasis. *Toxicon 45*, 1089–1098.
7. Leduc, M., and Bon, C. (1998) Cloning of subunits of convulxin, a collagen-like platelet-aggregating protein from *Crotalus durissus terrificus* venom. *Biochem. J. 333* (Part 2), 389–393.
8. Murakami, M. T., Zela, S. P., Gava, L. M., Michelan-Duarte, S., Cintra, A. C., and Arni, R. K. (2003) Crystal structure of the platelet activator convulxin, a disulfide-linked α4β4 cyclic tetramer from the venom of *Crotalus durissus terrificus*. *Biochem. Biophys. Res. Commun. 310*, 478–482.
9. Batuwangala, T., Leduc, M., Gibbins, J. M., Bon, C., and Jones, E. Y. (2004) Structure of the snake-venom toxin convulxin. *Acta Crystallogr., Sect. D: Biol. Crystallogr. 60*, 46–53.
10. Jandrot-Perrus, M., Lagrue, A. H., Okuma, M., and Bon, C. (1997) Adhesion and activation of human platelets induced by convulxin involve glycoprotein VI and integrin α2β1. *J. Biol. Chem. 272*, 27035–27041.
11. Polgar, J., Clemetson, J. M., Kehrel, B. E., Wiedemann, M., Magnenat, E. M., Wells, T. N., and Clemetson, K. J. (1997) Platelet activation and signal transduction by convulxin, a C-type lectin from *Crotalus durissus terrificus* (tropical rattlesnake) venom via the p62/GPVI collagen receptor. *J. Biol. Chem. 272*, 13576–13583.
12. Prado-Franceschi, J., and Brazil, O. V. (1981) Convulxin, a new toxin from the venom of the South American rattlesnake *Crotalus durissus terrificus*. *Toxicon 19*, 875–887.
13. Niedergang, F., Alcover, A., Knight, C. G., Farndale, R. W., Barnes, M. J., Francischetti, I. M., Bon, C., and Leduc, M. (2000) Convulxin binding to platelet receptor GPVI: competition with collagen related peptides. *Biochem. Biophys. Res. Commun. 273*, 246–250.
14. Horii, K., Kahn, M. L., and Herr, A. B. (2006) Structural basis for platelet collagen responses by the immune-type receptor glycoprotein VI. *Blood 108*, 936–942.
15. Gomes, M. M., Wall, S. B., Takahashi, K., Novak, J., Renfrow, M. B., and Herr, A. B. (2008) Analysis of IgA1 N-glycosylation and its contribution to FcαRI binding. *Biochemistry 47*, 11285–11299.
16. Herr, A. B., White, C. L., Milburn, C., Wu, C., and Bjorkman, P. J. (2003) Bivalent binding of IgA1 to FcαRI suggests a mechanism for cytokine activation of IgA phagocytosis. *J. Mol. Biol. 327*, 645–657.
17. Schuck, P. (2000) Size-distribution analysis of macromolecules by sedimentation velocity ultracentrifugation and Lamm equation modeling. *Biophys. J. 78*, 1606–1619.
18. Herr, A. B., Ornitz, D. M., Sasisekharan, R., Venkataraman, G., and Waksman, G. (1997) Heparin-induced self-association of fibroblast growth factor-2. Evidence for two oligomerization processes. *J. Biol. Chem. 272*, 16382–16389.
19. Myszka, D. G., and Morton, T. A. (1998) CLAMP: a biosensor kinetic data analysis program. *Trends Biochem. Sci. 23*, 149–150.
20. Alexander-Brett, J. M., and Fremont, D. H. (2007) Dual GPCR and GAG mimicry by the M3 chemokine decoy receptor. *J. Exp. Med. 204*, 3157–3172.
21. Svitel, J., Boukari, H., Van Ryk, D., Willson, R. C., and Schuck, P. (2007) Probing the functional heterogeneity of surface binding sites by analysis of experimental binding traces and the effect of mass transport limitation. *Biophys. J. 92*, 1742–1758.
22. Mizuno, H., Fujimoto, Z., Atoda, H., and Morita, T. (2001) Crystal structure of an anticoagulant protein in complex with the Gla domain of factor X. *Proc. Natl. Acad. Sci. U.S.A. 98*, 7230–7234.
23. Grucza, R. A., Bradshaw, J. M., Mitaxov, V., and Waksman, G. (2000) Role of electrostatic interactions in SH2 domain recognition: salt-dependence of tyrosyl-phosphorylated peptide binding to the tandem SH2 domain of the Syk kinase and the single SH2 domain of the Src kinase. *Biochemistry 39*, 10072–10081.
24. Record, M. T., Jr., Lohman, M. L., and De Haseth, P. (1976) Ion effects on ligand-nucleic acid interactions. *J. Mol. Biol. 107*, 145–158.
25. Du, X. Y., Clemetson, J. M., Navdaev, A., Magnenat, E. M., Wells, T. N., and Clemetson, K. J. (2002) Ophioluxin, a convulxin-like C-type lectin from *Ophiophagus hannah* (King cobra) is a powerful platelet activator via glycoprotein VI. *J. Biol. Chem. 277*, 35124–35132.
26. Tomlinson, M. G., Calaminus, S. D., Berlanga, O., Auger, J. M., Bori-Sanz, T., Meyaard, L., and Watson, S. P. (2007) Collagen promotes sustained glycoprotein VI signaling in platelets and cell lines. *J. Thromb. Haemostasis 5*, 2274–2283.
27. Zheng, Y. M., Liu, C., Chen, H., Locke, D., Ryan, J. C., and Kahn, M. L. (2001) Expression of the platelet receptor GPVI confers

signaling via the Fc receptor gamma-chain in response to the snake venom convulxin but not to collagen. *J. Biol. Chem. 276*, 12999–13006.
28. Chen, H., and Kahn, M. L. (2003) Reciprocal signaling by integrin and nonintegrin receptors during collagen activation of platelets. *Mol. Cell. Biol. 23*, 4764–4777.
29. Arthur, J. F., Shen, Y., Kahn, M. L., Berndt, M. C., Andrews, R. K., and Gardiner, E. E. (2007) Ligand binding rapidly induces disulfide-dependent dimerization of glycoprotein VI on the platelet plasma membrane. *J. Biol. Chem. 282*, 30434–30441.
30. Berlanga, O., Bori-Sanz, T., James, J. R., Frampton, J., Davis, S. J., Tomlinson, M. G., and Watson, S. P. (2007) Glycoprotein VI oligomerization in cell lines and platelets. *J. Thromb. Haemostasis 5*, 1026–1033.
31. Francischetti, I. M., Saliou, B., Leduc, M., Carlini, C. R., Hatmi, M., Randon, J., Faili, A., and Bon, C. (1997) Convulxin, a potent platelet-aggregating protein from *Crotalus durissus terrificus* venom, specifically binds to platelets. *Toxicon 35*, 1217–1228.
32. Kato, K., Furihata, K., Cheli, Y., Radis-Baptista, G., and Kunicki, T. J. (2006) Effect of multimer size and a natural dimorphism on the binding of convulxin to platelet glycoprotein (GP)VI. *J. Thromb. Haemostasis 4*, 1107–1113.
33. Miura, Y., Takahashi, T., Jung, S. M., and Moroi, M. (2002) Analysis of the interaction of platelet collagen receptor glycoprotein VI (GPVI) with collagen. A dimeric form of GPVI, but not the monomeric form, shows affinity to fibrous collagen. *J. Biol. Chem. 277*, 46197–46204.
34. Comeau, S. R., Gatchell, D. W., Vajda, S., and Camacho, C. J. (2004) ClusPro: an automated docking and discrimination method for the prediction of protein complexes. *Bioinformatics 20*, 45–50.
35. Dumont, B., Minullina, I., Loyau, S., Monteiro, R. C., Lacapere, J. J., Arocas, V., and Jandrot-Perrus, M. (2006) Chimeric Fc receptors identify ligand binding regions in human glycoprotein VI. *J. Mol. Biol*.
36. Kanaji, S., Kanaji, T., Furihata, K., Kato, K., Ware, J. L., and Kunicki, T. J. (2003) Convulxin binds to native, human glycoprotein Ib alpha. *J. Biol. Chem. 278*, 39452–39460.
37. Jarvis, G. E., Raynal, N., Langford, J. P., Onley, D. J., Andrews, A., Smethurst, P. A., and Farndale, R. W. (2008) Identification of a major GpVI-binding locus in human type III collagen. *Blood 111*, 4986–4996.
38. Orgel, J. P., Irving, T. C., Miller, A., and Wess, T. J. (2006) Microfibrillar structure of type I collagen in situ. *Proc. Natl. Acad. Sci. U.S.A. 103*, 9001–9005.
39. Herr, A. B., and Farndale, R. W. (2009) Structural insights into the interactions between platelet receptors and fibrous collagen, manuscript in preparation.

BI801820Q